Adenine and 2-aminopurine: Paradigms of modern theoretical photochemistry

Luis Serrano-Andrés[†‡], Manuela Merchán[†], and Antonio C. Borin[§]

[†]Instituto de Ciencia Molecular, Universitat de València, Dr. Moliner 50, Burjassot, ES-46100 Valencia, Spain; and [§]Instituto de Química, Universidade de São Paulo, Av. Prof. Lineu Prestes 748, SP 05508-900, São Paulo, Brazil

Communicated by Josef Michl, University of Colorado, Boulder, CO, April 15, 2006 (received for review October 18, 2005)

Distinct photophysical behavior of nucleobase adenine and its constitutional isomer, 2-aminopurine, has been studied by using quantum chemical methods, in particular an accurate *ab initio* multiconfigurational second-order perturbation theory. After light irradiation, the efficient, ultrafast energy dissipation observed for nonfluorescent 9H-adenine is explained here by the nonradiative internal conversion process taking place along a barrierless reaction path from the initially populated $^1(\pi\pi^*\ L_a)$ excited state toward a low-lying conical intersection (CI) connected with the ground state. In contrast, the strong fluorescence recorded for 2-aminopurine at 4.0 eV with large decay lifetime is interpreted by the presence of a minimum in the $^1(\pi\pi^*\ L_a)$ hypersurface lying below the lowest CI and the subsequent potential energy barrier required to reach the funnel to the ground state. Secondary deactivation channels were found in the two systems related to additional CIs involving the $^1(\pi\pi^*\ L_b)$ and $^1(n\pi^*)$ states. Although in 9H-adenine a population switch between both states is proposed, in 7H-adenine this may be perturbed by a relatively larger barrier to access the $^1(n\pi^*)$ state, and, therefore, the $^1(\pi\pi^*\ L_b)$ state becomes responsible for the weak fluorescence measured in aqueous adenine at ≈4.5 eV. In contrast to previous models that explained fluorescence quenching in adenine, unlike in 2-aminopurine, on the basis of the vibronic coupling of the nearby $^1(\pi\pi^*)$ and $^1(n\pi^*)$ states, the present results indicate that the $^1(n\pi^*)$ state does not contribute to the leading photophysical event and establish the prevalence of a model based on the CI concept in modern photochemistry.

conical intersections | DNA photophysics | fluorescence quenching | quantum chemistry | ultrafast decay

Studies on the photostability of DNA and RNA bases after absorption of UV light have flourished since the early 1970s, when quenched DNA fluorescence at room temperature was first reported (1). Knowledge about the mechanisms that control nonradiative decay is fundamental, not only because of the extreme importance of photodamage in systems that form the genetic code but also because they have been used to establish the paradigm of the essentials of radiationless decay processes in nonadiabatic photochemistry (2). Adenine (6-aminopurine), the most studied nucleobase, maintains photostability by efficiently quenching its fluorescence, whereas a close constitutional isomer, 2-aminopurine, displays strong emission, and it is commonly used to substitute adenine in DNA as a fluorescent probe to detect protein-induced local conformational changes (3–7). Former proposals to explain low quantum yields of fluorescence and excited singlet deactivation in nucleobases by means of excited-state photoreactions or phototautomerisms were basically ruled out because of the absence of photoproducts and deuterium isotope effects in different solvents (2). Apparently more successful was the hypothesis known as proximity effect (8, 9), which explained ultrafast internal conversion (IC) by vibronic coupling between the two low-lying and nearby $\pi\pi^*$ and $n\pi^*$ states found in this type of heteroaromatic molecules. The model used the energy difference between the excited states, typically known from the absorption spectra, to modulate the extent of the coupling: The smaller the gap is, the more efficient is the coupling between S_2/S_1 states. If the vibrational coupling taking place via low-frequency, out-of-plane accepting modes is large enough, the Franck–Condon (FC) factor associated with the radiationless transition is also large and leads to a rapid conversion to the ground-state hypersurface and, ultimately, to fast relaxation from high vibrational levels of the ground state, S_0. Lim's proximity effect (10) is frequently mentioned in the photochemical literature, and a number of theoretical studies, although using limited low-level methods, have tried to support the model and use it to explain the photochemistry of nucleobases (11–15). However, there is experimental evidence clearly questioning the validity of this oversimplified scheme, especially in the DNA/RNA bases, which have similar decays upon methylation or in polar solvents, where the $n\pi^*$ state vanishes or is highly perturbed (2). More important, the paradigm to explain nonadiabatic photochemistry and radiationless deactivation processes based on the role of conical intersections (CIs) between potential energy surfaces (PES) and founded on solid quantum chemical calculations seems to better rationalize the experimental findings. The current CI scheme is the result of complementary experimental and theoretical work by many authors in recent years (2, 16–23).

In modern photochemistry, the efficiency of radiationless decay between different electronic states taking place in IC and intersystem crossing processes is associated to the presence of crossings of different PES along a hyperline or hyperplane, i.e., an N-2 or N-1 dimensional subspace, respectively, on the N-dimensional surfaces. The points belonging to these subspaces or seams, that is, CIs and singlet/triplet crossings, behave as energy funnels where the probability for nonadiabatic, nonradiative jumps is high (18, 24, 25). The nature of the deactivation is certainly related with the strong vibronic coupling taking place between the interacting states when the energy gap decreases, in particular in situations such as CIs (19). The electronic excited state related to the transition with the largest absorption probability will in principle play the main role in the photochemistry of a given compound, together with the corresponding pathways leading to the lowest-excited S_1 state. In a static approach, the mechanism for the predominant, efficient deactivation to the ground state is ascribed to the regions where the most accessible S_1/S_0 CIs are located. Any retardation in the reaction rate reflects the presence of excited-state energy barriers. Fluorescence quantum yields and excited-state lifetimes, therefore, can be related to the nature of the paths and the barriers that the system has to surmount to reach the crossing seam, or, more loosely, its minimal-energy crossing point, that is, the lowest-energy S_1/S_0 CI. Introduced a decade ago as the photochemical reaction path approach (26), the theoretical strategy based on mapping the path for the efficient transit of energy in excited states toward the accessible CIs using highly accurate quantum chemical methods certainly provides the key parameters to understand the photo-

Conflict of interest statement: No conflicts declared.

Abbreviations: IC, internal conversion; CI, conical intersection; FC, Franck–Condon; PES, potential energy surface(s); MEP, minimum energy path; CASPT2, multiconfigurational second-order perturbation theory; CASSCF, complete active space self-consistent field.

[‡]To whom correspondence should be addressed. E-mail: luis.serrano@uv.es.

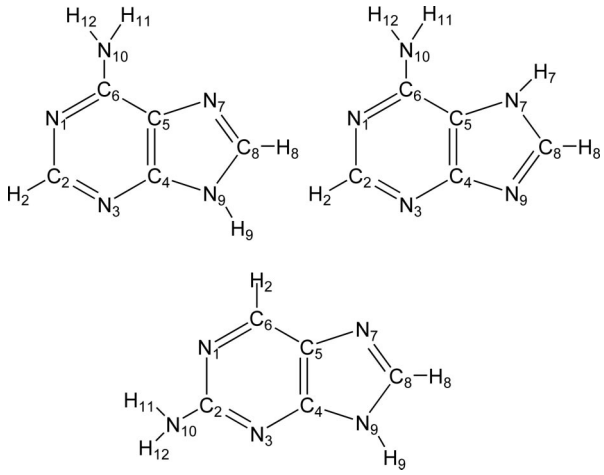

Fig. 1. Structure and atom labeling for 9H-adenine (*Upper Left*), 7H-adenine (*Upper Right*), and 9H-2-aminopurine (*Lower*).

chemical mechanisms and forms the basis for future theoretical studies on the dynamics of the system that may ultimately lead to the prediction of the time evolution of the process. In the present contribution, we illustrate the importance of a quantum chemical description of PES based on the computation of state minima, barrier heights, CIs, and, in particular, the proper calculation of minimum energy paths (MEPs) connecting the singular points in a way that allows us to carefully determine the most favorable paths for the energetic decay and understand the different behavior of systems as adenine and 2-aminopurine.

Previous theoretical studies, pioneered by Ismail *et al.* (27), suggested the importance of CIs as responsible for ultrafast IC in the DNA bases, but the determination of its structure and nature has been controversial. Recently, the main role in the ultrafast relaxation of the nucleobases of low-energy CIs between the ground and a low-lying $^1(\pi\pi^*)$ state has been established in cytosine, uracil, and adenine, whereas other states ($n\pi^*$, $\pi\sigma^*$) have been proposed to contribute to the different decay pathways (28–35). Particularly relevant and valuable for the present work are recent multiconfigurational second-order perturbation theory (CASPT2) studies on adenine (34, 35) and the analyses of several structures of adenine and 2-aminopurine at the density functional theory /multireference configuration interaction level (33, 36). The most recent evidence highlights the relevance of out-of-plane distortions in all nucleobases (31, 33–35). To rationalize the different photophysical behavior of adenine and 2-aminopurine (see Fig. 1), the present work has been undertaken. For this purpose, the main IC channels in adenine and 2-aminopurine have been determined by computing specific MEPs on the PES of their low-lying singlet excited states, by describing the lowest relaxation pathways for the energy, and by locating the most accessible CIs and energy barriers. In a previous study (35), several aspects of the photophysics of adenine tautomers and derivatives were considered. Here we will focus on the careful comparison of the photophysics of adenine and 2-aminopurine, stressing similarities and discrepancies. The current scheme, based on a three-state model for these compounds, explains why adenine displays just a weak fluorescence, dissipating most of the absorbed energy by ultrafast, radiationless IC processes detected in the femtosecond and picosecond ranges (37, 38), whereas 2-aminopurine fluorescence can actually be recorded and is much more intense and is near 0.7 eV lower in energy (39, 40). The different properties of adenine and 2-aminopurine upon absorption of radiation make them good candidates to check the reliability of the models and mechanisms under study. CASPT2//complete active space self-consistent field (CASSCF) energy paths and profiles will be used to rationalize the photophysics of both compounds on the basis of their relaxation pathways from the initially excited singlet state and establish the prevalence of a model based on the CI concept.

Results and Discussion

Why 2-Aminopurine Is Highly Fluorescent, Whereas Adenine (6-Aminopurine) Is Not. 2-Aminopurine behaves as a highly emissive source. Measurements in water provided a fluorescence band origin at 3.70 eV (41) and a emission quantum yield (ϕ_F) of 0.66 (39, 40). A single-component fluorescence decay, with a large lifetime between 9.3 and 11.8 ns, was reported and assigned to the 9H-tautomer (6, 39, 42–44). Solvent polarity definitively favors emission, because, in the close derivative 9-ethyl-2-aminopurine, ϕ_F varies from 0.010 in the nonpolar solvent cyclohexane to 0.68 in water (45). On the contrary, it was reported that emission is efficiently quenched in adenine, and this basic photophysical behavior is maintained in solution (1). An extremely weak fluorescence with low quantum yield, $\phi_F = 2.9 \times 10^{-4}$ to 3.3×10^{-4}, is detected starting at 4.43 eV in aqueous environments (2, 46–51). Two decay lifetimes have been measured in solution, depending on the different techniques and wavelengths used: the ultrafast decay from 180 to 670 fs and the slower relaxation from 8.4 to 8.8 ps (2). At least two decay channels also have been measured in jet-cooled adenine after irradiation at 250 or 267 nm (4.95 and 4.64 eV, respectively), corresponding to a double exponential decay: $<$100 fs and 1.1 ps (37, 38). Therefore, the experimental evidence points out that adenine finds efficient ways to dissipate the absorbed energy different from emission.

According to Lim's proximity effect model (8–10), the two close, lowest-lying $\pi\pi^*$ and $n\pi^*$ excited states were supposed to interact, coupling through certain low-energy, out-of-plane vibrational distortions, which ultimately led to an increasing overlap with the ground state vibration and large FC factors favoring radiationless IC to the ground state. Many of those conclusions are based on observed or computed vertical energy gaps between the states (11, 52), with emphasis on the fact that in adenine a small energy gap is found between the lowest $\pi\pi^*$ and $n\pi^*$ excited states, whereas in 2-aminopurine the lowest $\pi\pi^*$ state is much lower in energy and cannot interact with the $n\pi^*$ state properly.

Table 1 compiles relevant experimental data together with our computed CASPT2 values. Although the present study is focused on the major 9H-tautomer both for 2-aminopurine and adenine, some aspects of the photophysics of 7H-adenine also are analyzed, considering that it has distinct photophysics that influence measurements in polar media, unlike 2-aminopurine, in which the photophysics of both tautomers seems to be quite similar (43). 2-Aminopurine displays absorption maxima in stretched poly(vinyl alcohol) films (39) peaking at 4.1 (0.10), 4.5 (0.002), and 5.1 eV (0.07), where the oscillator strengths have been included in parentheses. Transition to three low-lying, singlet, excited states have been computed vertically at 4.33 (0.070), 4.46 (0.008), and 5.33 eV (0.148) at the CASPT2 level, in relative accordance with the experimental data. The features are assigned to the $^1(\pi\pi^*\ L_a)$, $^1(n\pi^*)$, and $^1(\pi\pi^*\ L_b)$ transitions, respectively. Platt's nomenclature (53) allows us to distinguish between the two low-lying $\pi\pi^*$ states: $^1(\pi\pi^*\ L_a)$ is described mainly (36%) by the highest occupied molecular orbital (H)→lowest unoccupied molecular orbital (L) one-electron promotion, whereas the $^1(\pi\pi^*\ L_b)$ state wave function is basically formed by a linear combination (20% each) of two configurations, H→L + 1 and H − 1→L. The intensity of the bands in the low-energy range of the absorption spectra of 2-aminopurine seems to be distributed between the two $^1(\pi\pi^*)$ transitions. Regarding band origins, the resonant two-photon ionization spectrum of 2-aminopurine in the gas phase displayed an extended vibronic structure, with a band origin (T_0) for the recorded lowest-lying state at 4.01 eV (36, 52), red-shifted 0.5 eV below the corresponding feature in adenine. The band origin in water is red-shifted to ≈3.70 eV (41). Our computed value of 3.89 eV for the adiabatic origin of the $^1(\pi\pi^*\ L_a)$ state clearly agrees with the observed data in the

Table 1. Computed properties for the low-lying singlet excited states of 9H-adenine, 7H-adenine, and 9H-2-aminopurine at the CASPT2//CASSCF(16/13)/6-31G(d,p) level

	Absorption					Band origin/emission properties			
	Theory			Experiment		Theory		Experiment	
State	ΔE, eV	f	μ, D	ΔE, eV	f	T_e, eV	τ_{rad}, ns	T_0, eV	τ_{rad}, ns
9H-adenine									
^{1}(gs)			2.67						
$^1(n\pi^*)$	4.96	0.004	1.99	—	—	4.52	334	4.40[†]	—
$^1(\pi\pi^*\ L_b)$	5.16	0.004	2.46	4.6[‡]	0.08[‡]	4.83	251	4.48[†]	—
$^1(\pi\pi^*\ L_a)$[§]	5.35	0.175	4.17	5.0[‡]	0.2[‡]				
7H-adenine									
^{1}(gs)			6.35						
$^1(n\pi^*)$	4.74	0.009	4.14	—	—	4.14	177	—	—
$^1(\pi\pi^*\ L_b)$	5.06	0.022	5.38	—	—	4.60	54	4.43[¶]	34[¶]
$^1(\pi\pi^*\ L_a)$[§]	5.41	0.072	8.38	—	—				
9H-2-aminopurine									
^{1}(gs)			3.14						
$^1(\pi\pi^*\ L_a)$	4.33	0.070	3.19	4.1[‖]	0.10[‖]	3.89	25	4.01[††]	18[††]
$^1(n\pi^*)$	4.46	0.008	3.54	4.5[‖]	0.002[‖]	4.04	138	—	—
$^1(\pi\pi^*\ L_b)$	5.33	0.148	3.16	5.1[‖]	0.07[‖]	4.84	7	—	—

—, not reported.

[†]Absorption band origins for jet-cooled adenine, assigned to 9H-adenine (54–58).

[‡]Absorption band maxima in adenine (47, 59–61).

[§]Geometry optimization leads to $(gs/\pi\pi^*\ L_a)_{CI}$ in adenine (see *Results and Discussion* and ref. 35).

[¶]Absorption band origin for jet-cooled adenine and fluorescence in water (both assigned to 7H-adenine): $\phi_F = 2.6 \times 10^{-4}$, $\tau_F = 8.8$ ps, $\tau_{rad} = \tau_F/\phi_F$ (47, 48).

[‖]Absorption band maxima for 2-aminopurine in poly(vinyl alcohol) films (39) and in water (40).

[††]Jet-cooled 9H-2-aminopurine. Fluorescence in water: $T_0 = 3.70$ eV (41), $\phi_F = 0.66$, $\tau_F = 11.8$ ns, $\tau_{rad} = \tau_F/\phi_F$ (39)

vapor, whereas our calculated radiative lifetime (τ_{rad}), 25 ns, falls within the order of magnitude of the experimental value, 18 ns, estimated from quantum yields and intrinsic lifetimes in water (39). We also computed the minima of the $^1(n\pi^*)$ and $^1(\pi\pi^*\ L_b)$ states, leading to band origins at 4.04 and 4.84 eV, respectively. On the basis of these results, we can confirm that the observed fluorescence in 2-aminopurine starting at 4.01 eV in the gas phase and peaking near 3.4 eV in water (39, 41) takes place from the $^1(\pi\pi^*\ L_a)$ state but also that the origin of the $^1(n\pi^*)$ state is above the $^1(\pi\pi^*\ L_a)$ origin by $\approx$0.1 eV. A similar gap was estimated in jet-cooled adenine for the equivalent band origins (54–58), whereas for the vertical values the computed energy difference even increases (compare with Table 1) (35, 46–48, 59–61). It is therefore clear that both 9H-adenine and 9H-2-aminopurine have close-lying $^1(\pi\pi^*\ L_a)$ and $^1(n\pi^*)$ states, although their photophysical behavior drastically differs. The energy gap criterion is certainly not solid enough to sustain the proximity effect model.

To understand photoinduced processes, the evolution pathways with respect to the relevant reaction coordinates have to be known. We have therefore computed MEPs along the most relevant singlet excited states of the molecules. Fig. 2 displays the energies of the low-lying singlet excited states of 9H-2-aminopurine computed at the CASPT2 level from the FC ground-state geometry along the CASSCF MEP on the $^1(\pi\pi^*\ L_a)$ hypersurface, followed by a reaction path through a transition state and a CI with the ground state. When directly populated, the H→L $^1(\pi\pi^*\ L_a)$ state is the lowest one at all geometries (see also Table 2), whereas the $^1(\pi\pi^*\ L_b)$ state is placed energetically too high to be of primary photophysical importance. The $^1(\pi\pi^*\ L_a)$ state evolves from the FC structure to an almost planar minimum, $^1(\pi\pi^*\ L_a)_{min}$. From that region, the system has to release the energy either by emitting radiation or by reaching a higher-lying CI, $(gs/\pi\pi^*\ L_a)_{CI}$, by surmounting a barrier of 5.0 kcal·mol^{-1} through an intermediate transition state, $^1(\pi\pi^*\ L_a)_{TS}$ (see Fig. 2). As it was discussed previously, the computed band origin for the $^1(\pi\pi^*\ L_a)$ state, 3.89 eV, matches quite well the experimental measurement, 4.01 eV. Initially, the deformation leading from the FC region to the minimum involved an enlargement of the N_1C_2 and C_2C_3 bonds, which can be understood by analyzing the change for these bonds from a bonding to an antibonding character in the H and L orbitals, respectively. From the minimum, the out-of-plane vibrational modes leading to the basic deformation at the CI involve the twisting of the N_3C_2 bond, moving the amino group to a perpendicular disposition (dihedral angle $C_6C_1C_2N_2$) with respect to the rings, a structure that represents a large distortion when evolving from the almost planar $^1(\pi\pi^*\ L_a)$ minimum.

The same strategy to compute $^1(\pi\pi^*\ L_a)$ MEPs was followed in 9H- and 7H-adenine (35). In the major 9H-tautomer, the obtained path after crossing the $^1(n\pi^*)$ and $^1(\pi\pi^*\ L_b)$ states' PES at high energies leads directly to a CI with the ground state, $(gs/\pi\pi^*\ L_a)_{CI}$. The path has a steepest-descendent nature and, consequently, the $^1(\pi\pi^*\ L_a)$ state has no minimum (see Fig. 3). This feature is the corner stone of adenine photochemistry. Taking into consideration

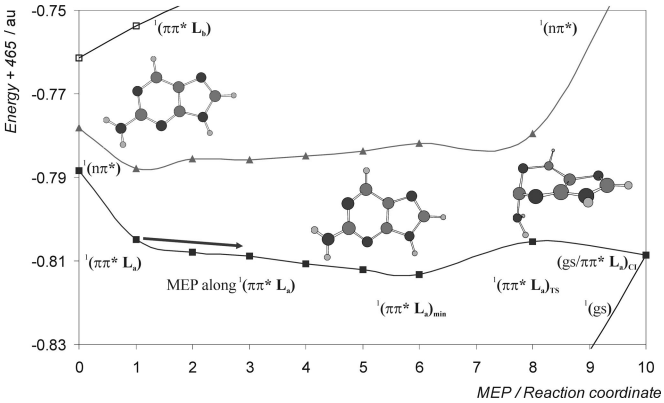

Fig. 2. Low-lying singlet excited states of 9H-2-aminopurine computed at the CASPT2//CASSCF level from the FC ground-state geometry along the MEP on the $^1(\pi\pi^*\ L_a)$ state [up to $^1(\pi\pi^*\ L_a)_{min}$] and along the reaction coordinate including $^1(\pi\pi^*\ L_a)_{TS}$ and $(gs/\pi\pi^*\ L_a)_{CI}$.

Table 2. Computed CI structures and energy barriers (kcal·mol^{-1}) for the low-lying singlet excited states of 9H-adenine and 9H-2-aminopurine at the CASPT2//CASSCF(12,11)/ 6-31G(d,p) level

Structure	9H-adenine		9H-2-aminopurine	
	ΔE_1	ΔE_2	ΔE_1	ΔE_2
$(gs/\pi\pi^* L_a)_{CI}$	—	0.0[†]	2.9	0.0[†]
$(gs/n\pi^*)_{CI}$	1.6	11.7	0.9	1.2
$(\pi\pi^* L_b/n\pi^*)_{CI}$	3.2/11.6	21.7	—	—
$(\pi\pi^* L_b/\pi\pi^* L_a)_{CI}$	5.3/—	23.8	4.3/25.9	23.0
$(n\pi^*/\pi\pi^* L_a)_{CI}$	19.8/—	29.9	7.0/10.2	7.3
$(n\pi^*)_{TS}$[‡]	1.9	12.0	1.9	2.2
$(\pi\pi^* L_a)_{TS}$[§]	—	—	5.0	2.1

Minima and transition states computed at the CASPT2//CASSCF level. CIs were computed from CASPT2 results. ΔE_1 denotes the energy barrier from the excited state minima to the computed CIs or transition states, and ΔE_2 denotes the energy difference between the corresponding CIs or transition states and the reference $(gs/\pi\pi^* L_a)_{CI}$ energy. —, not applicable.

[†]At this level the CI is placed adiabatically with respect to the ground state at 4.09 eV (9H-adenine) and 4.12 eV (9H-2-aminopurine).

[‡]Transition state connecting $(n\pi^*)_{min}$ with $(gs/n\pi^*)_{CI}$.

[§]Transition state connecting $(\pi\pi^* L_a)_{min}$ with $(gs/\pi\pi^* L_a)_{CI}$.

that upon light irradiation the $^1(\pi\pi^* L_a)$ state has the major population, the energy will be deactivated to the ground state through the CI $(gs/\pi\pi^* L_a)_{CI}$ in an efficient, ultrafast, nonradiative IC process that quenches most of the fluorescence. The initial downhill profile of the L_a PES in 9H-adenine is equivalent to the one found for 9H-2-aminopurine. As in 9H-2-aminopurine, it is the twisting and wagging of the N_3C_2 bond that ultimately leads to the CI $(gs/\pi\pi^* L_a)_{CI}$, although in adenine it is just an hydrogen atom bonded to C_2 that becomes perpendicular to the rings (see dihedral angle $C_6C_1C_2H_2$ in Fig. 3). The out-of-plane deformation generating the CI structures is characterized by coupled torsional and wagging motions of the center's substituent (either H in adenine or NH_2 in 2-aminopurine). Unlike in 2-aminopurine, where the wagging of the amino group was forced, in adenine the distortion implies out-of-plane modes involving the H_2 atom, and there is no barrier hindering the access to the CI and therefore preventing the ultrafast nonradiative decay. Differently, in 7H-adenine, the computed path leads to a local minimum on the $^1(\pi\pi^* L_a)$ hypersurface, $^1(\pi\pi^* L_a\ NH_2)_{min}$, having a planar conformation for the rings while the NH_2 hydrogen atoms are twisted near 60° and the amino nitrogen lone-pair electrons face hydrogen H_7 (see *Supporting Methods*, which is published as supporting information on the PNAS web site). The character of the state remains the same, however; that is, the $\pi\pi^*$ excitation is restricted to the rings without charge transfer from the NH_2 moiety. The PES around the region

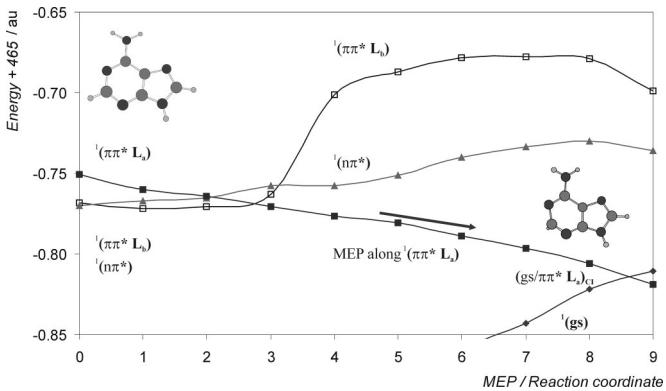

Fig. 3. Low-lying singlet excited states of 9H-adenine computed at the CASPT2//CASSCF level from the FC ground-state geometry along the MEP on the $^1(\pi\pi^* L_a)$ state.

of the $^1(\pi\pi^* L_a\ NH_2)_{min}$ minimum is quite flat for the three computed singlet excited states, which become almost degenerate and cross at energies similar to those computed in 9H-adenine. From those crossings, one can expect that part of the energy can reach the minima of the $^1(n\pi^*)$ and $^1(\pi\pi^* L_b)$ states along their respective paths.

One basic difference, therefore, can be expected in the photophysics of both adenine tautomers. Although in 9H-adenine most of the energy will be quickly transferred to the ground state via a barrierless path along the $^1(\pi\pi^* L_a)$ PES and through the CI $(gs/\pi\pi^* L_a)_{CI}$, explaining the observed ultrafast decays (<100 fs) in 9H-adenine and 9-methyladenine (38), in 7H-adenine the presence of the $^1(\pi\pi^* L_a\ NH_2)_{min}$ minimum represents a barrier to surmount, hindering the fast relaxation. No equivalent ultrafast decay has been measured in 7-methyladenine (62, 63), and we may attribute this absence to the profile of the reaction path itself, together with the fact that part of the population may be transferred to the $^1(n\pi^*)$ and $^1(\pi\pi^* L_b)$ states in the region of the plateau. Because of this feature, the 7H-tautomer can contribute to the emitting properties of adenine in solution, as it is explained in *Secondary Pathways to Dissipate the Energy*.

Fig. 4 summarizes the basics of the photophysics of 9H-adenine and 9H-2-aminopurine designed on the basis of the present calculations. Regarding the main relaxation paths of the molecules, both mechanisms relate with the spectroscopic $^1(\pi\pi^* L_a)$ states, and their profiles account for the different emissive properties. In 9H-2-aminopurine, the path from the minimum of the $^1(\pi\pi^* L_a)$ state to reach the lowest CI has a computed barrier of 5.0 kcal·mol^{-1}, and the CI lies above the minimum. The theoretical results are consistent with the measured fluorescence and the corresponding slow decay, reported in water with a lifetime 11.8 ns. On the contrary, in 9H-adenine, the analogous $^1(\pi\pi^* L_a)$ state has no minimum, and the lowest-lying, singlet excited state structure corresponds to a CI that allows relaxation of the system toward the ground state in a barrierless, ultrafast (subpicosecond) manner. Fluorescence is surely enhanced in polar media (45) for 2-aminopurine because of the larger stabilization of the $^1(\pi\pi^* L_a)_{min}$ structure in polar solvents, as compared with the barrier or the CI. Elucidation of the effects of the solvent on the PES profiles will require a more detailed theoretical study.

Secondary Pathways to Dissipate the Energy. We have shown that reaction paths related to the $^1(\pi\pi^* L_a)$ state form the primary mechanism for energy relaxation as a fluorescent source in 9H-2-aminopurine and in a radiationless way in 9H-adenine. Secondary relaxation mechanisms can be found along the other low-lying singlet states PES. Table 2 and Fig. 4 summarize the computed structures and the energy barriers required to reach the PES funnels.

In 9H-2-aminopurine, the $^1(n\pi^*)$ state lies vertically slightly above the $^1(\pi\pi^* L_a)$ state, and it will not be largely populated by direct absorption considering the almost forbidden character of the corresponding transition. A CI between the two states, $(\pi\pi^* L_a/n\pi^*)_{CI}$, at a nearly planar structure, intermediate between the FC geometry and the $^1(n\pi^*)$ minimum conformation, has been found, however, and it may lead to a partial population switch toward the low-lying $^1(\pi\pi^* L_a)$ state. From the slightly distorted $^1(n\pi^*)$ state minima, $^1(n\pi^*)_{min}$ (see Fig. 4), it also is possible to reach a CI with the ground state, $(gs/n\pi^*)_{CI}$, having a structure in which the N_1C_6 bond has been twisted, leaving H_2 perpendicular to the rings. The barrier to access the CI from $^1(n\pi^*)_{min}$ through the transition state structure, $^1(n\pi^*)_{TS}$, has been computed at 1.9 kcal·mol^{-1} above the minimum. In the gas phase, there is enough excess vibrational energy to surmount the barrier, and the expected lifetimes should not be too large. In polar environments, however, the $^1(n\pi^*)$ state clearly will be destabilized, and the profile will change accordingly, probably increasing the relaxation times.

Regarding the higher-lying $^1(\pi\pi^* L_b)$ state, a CI has been

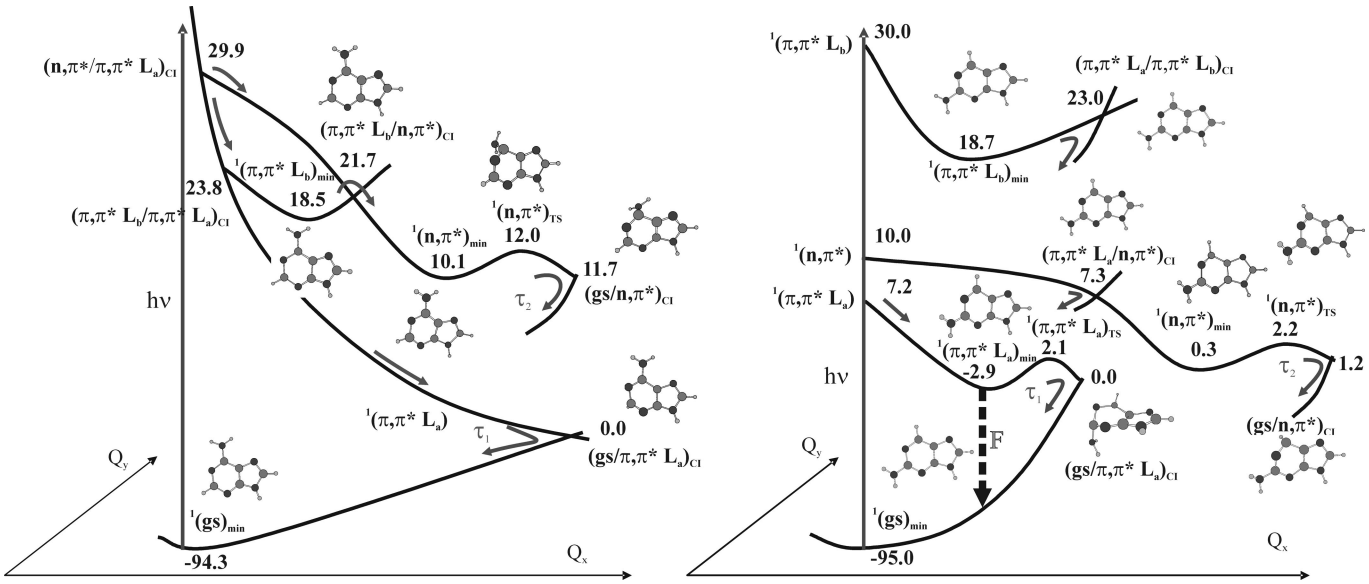

Fig. 4. Scheme based on CASPT2 calculations for the main decay pathways of 9H-adenine (*Left*), measured in molecular beams with intrinsic lifetimes $\tau_1 < 100$ fs and $\tau_2 \approx 1$ ps (38), and 9H-2-aminopurine (*Right*), displaying water-intense fluorescence ($\phi_F = 0.66$) and large lifetimes (39, 40). Energies in kcal·mol^{-1} refer to the lowest (gs/$\pi\pi^*$) CI.

computed connecting the two low-lying $^1(\pi\pi^*)$ states, ($\pi\pi^*$ L_a/$\pi\pi^*$ $L_b)_{CI}$, placed 4.3 kcal·mol^{-1} above the $^1(\pi\pi^*$ $L_b)$ state minimum, $^1(\pi\pi^*$ $L_b)_{min}$. Taking into account the large oscillator strength calculated for the $^1(\pi\pi^*$ $L_b)$ vertical transition, such a funnel may become important when the system is irradiated with a short wavelength to additionally populate the $^1(\pi\pi^*$ $L_a)$ state and so contribute to the final fluorescence. Recent transient–absorption experiments in aqueous environments (64) identified three low-lying excited states in 2-aminopurine. A nonfluorescent long-lived state that we assign as $^1(n\pi^*)$, with excited-state absorption polarized perpendicular to the ground-state absorption, was detected in minor proportion and decayed with a lifetime of >15 ns (64), a channel that also has been attributed to other species (43). In contrast, another state displaying stimulated emission was measured, and it evolved in 1.3 ps into a new fluorescent state that finally decays in ≈6.5 ns (64). According to the present results, the two pathways can be related to the $^1(\pi\pi^*$ $L_b)$ and $^1(\pi\pi^*$ $L_a)$ states of 9H-2-aminopurine, respectively, whereas the computed CIs connecting both states and finally the ground state represent the funnels for efficient IC.

With respect to 9H-adenine and along the MEPs of the $^1(\pi\pi^*$ $L_a)$ state, a fraction of the population can be transferred to the $^1(n\pi^*)$ and $^1(\pi\pi^*$ $L_b)$ routes mediated by the CIs ($n\pi^*/\pi\pi^*$ $L_a)_{CI}$ and ($\pi\pi^*$ $L_b/\pi\pi^*$ $L_a)_{CI}$ toward their respective minima (compare with Fig. 4) (35). The $^1(\pi\pi^*$ $L_b)$ state minima also can be populated by direct absorption (54–58), in particular in 7H-adenine, in which transition to $^1(\pi\pi^*$ $L_b)$ is computed with a relatively larger oscillator strength. From $^1(\pi\pi^*$ $L_b)_{min}$, the MEP shows a barrier to reach the CI with the $^1(n\pi^*)$ state, 3.2 kcal·mol^{-1} above $^1(\pi\pi^*$ $L_b)_{min}$ in 9H-adenine, and 7.6 kcal·mol^{-1} in 7H-adenine (35). Therefore, because of the presence of the barrier and, consequently, the corresponding decrease in the excess of vibrational energy available to reach the CI, one could expect a longer lifetime associated to this decay when the $^1(\pi\pi^*$ $L_b)$ state band origin would become directly populated. Indeed, this assumption has been corroborated experimentally. At long excitation wavelengths [277 nm (4.48 eV)], a single decay has been measured with a lifetime of >2 ps (it was 1.1 ps at shorter wavelengths) (37). The fact that the barrier is larger in 7H-adenine, together with the profile of the $^1(\pi\pi^*$ $L_a)$ MEP in the 7H tautomer, including a plateau where an efficient population transfer from the $^1(\pi\pi^*$ $L_a)$ to the $^1(\pi\pi^*$ $L_b)$ degenerate states can take place (see Fig. 5, which is published as supporting information on the PNAS web site), leads us to suggest that the weak fluorescence ($\phi_F \approx 3 \times 10^{-4}$) observed in aqueous adenine starting near 4.43 eV (46, 52) comes essentially from the $^1(\pi\pi^*$ $L_b)$ state of the minor 7H-tautomer. This assignment is also confirmed by comparing the computed and measured radiative lifetimes (see Table 1) and by our calculated band origin at 4.60 eV, lower than for 9H-adenine, as discussed elsewhere (35). Experimental evidence also supports that 7-substituted adenines fluoresce more intensely than 9-substituted adenines, whereas adenine nucleoside and nucleotide (9-substituted species) are known to fluoresce less than the monomer (2, 46, 47).

Also in adenine, after the switch to the $^1(n\pi^*)$ state through the ($\pi\pi^*$ $L_b/n\pi^*)_{CI}$ CI, the $^1(n\pi^*)$ state minima can be reached through a reaction path similar to that computed for the equivalent state in 9H-2-aminopurine. A CI (gs/$n\pi^*)_{CI}$ can be accessed from $^1(n\pi^*)_{min}$ after surmounting a small barrier of 1.9 kcal·mol^{-1} through the transition state, $^1(n\pi^*)_{TS}$. The deformation leading to the CI is, like in 2-aminopurine, the rotation of the N_1C_6 bond. Here, however, the amino group, NH_2, substitutes C_6, and the associated normal modes leading to a NH_2 structure perpendicular to the ring structure have larger energy (see Figs. 6 and 7, which are published as supporting information on the PNAS web site). We tentatively propose that the path leading from $^1(\pi\pi^*$ $L_b)$ to the $^1(n\pi^*)$ state, finally reaching the CI with the ground state, (gs/$n\pi^*)_{CI}$, is responsible for the second, slower, relaxation decay measured in jet-cooled adenine with a lifetime of 1.1 ps (38). A piece of strong evidence in favor of such an assignment is the measured decay lifetimes in jet-cooled *N*,*N*-dimethyldenine: 200 fs and 3.1 ps (38). Although in this system the ultrafast decay remains similar to that in adenine because the deformation in the $N_3C_2H_2$ structure is equivalent, the second relaxation triples its lifetime in *N*,*N*-dimethyldenine, a logical consequence of the role of a relatively hindered (gs/$n\pi^*)_{CI}$ CI because of the presence of two methyl groups substituting N_1.

Final Remarks. Although adenine efficiently quenches fluorescence, 2-aminopurine (a similar molecule) is a highly emissive source used to probe protein-induced conformational changes in DNA. We have rationalized their different photophysical behavior by mapping the PES at the highest available theoretical level, *ab initio*

CASPT2, based on carefully computed MEPs, state minima, CIs, transition states, and barriers. A three-state model comes out for both systems, explaining (*i*) the strong fluorescence measured in 2-aminopurine because of the presence of a $^1(\pi\pi^*)$ state minimum below the lowest accessible CI; (*ii*) how in adenine a barrierless pathway from the initially populated excited state leads to the analogous CI and consequently to an efficient IC toward the ground state dissipating most of the energy; (*iii*) that the two observed decay mechanisms are mediated by two distinct CIs with the ground state; (*iv*) how the 7H-tautomer has a major contribution to the weak fluorescence recorded in solvated adenine.

Up to quite recently, a limited scheme like Lim's proximity effect model involving the coupling of nearby $\pi\pi^*$ and $n\pi^*$ states still has been claimed to explain quenching of fluorescence in these important systems. It has been shown here both in adenine and 2-aminopurine that the $n\pi^*$ states do not play an important role in the leading photophysical event, whereas the character, relative location, and accessibility of the lowest CI do. Until more elaborated theoretical studies including time scale can be performed in systems of this size using quantum chemical parameters, at least as accurate as the present ones, knowledge of the photochemical reaction path (i.e., MEP after the initial irradiation, minimum energy barriers required to access CIs, and crossing seams) represents the most powerful theoretical approach presently available to interpret photochemical processes.

Methods

Optimizations of minima, PES crossings, and MEPs have been performed at the CASSCF level of theory. MEPs have been built as steepest descendent paths in which each step requires the minimization of the PES on a hyperspherical cross section of the PES centered at the initial geometry and characterized by a predefined radius (see *Supporting Methods*). At the obtained points, CASPT2 calculations on several singlet states were carried out to include the necessary dynamical correlation effects. The protocol is usually named CASPT2//CASSCF and has proved its accuracy repeatedly (65–71). The CI searches were carried out first at the CASSCF level by obtaining minimum energy crossing points and later by performing CASPT2 calculations around the CASSCF-optimized structures. The one-electron atomic basis set 6–31G(d,p) was used throughout. Unless otherwise specified, the final results use an active space of 11 orbitals and 12 electrons. No symmetry restrictions were imposed during the calculations, which in all cases used the MOLCAS-6 set of programs (72). From the calculated CASSCF transition dipole moments and the CASPT2 excitation energies, the radiative lifetimes have been estimated by using the Strickler–Berg relationship (73), which is basically valid under the hypothesis that no excited-state deactivation occurs. A detailed description of additional technical details can be found in *Supporting Methods* and Tables 3–5, which are published as supporting information on the PNAS web site, together with the selected geometries computed for the different systems.

A.C.B. thanks the Brazilian Research Council, Fundaçaõ de Amparo à Pesquisa do Estado de São Paulo, and Universitat de València for financial support. This work was supported by Ministerio de Educación y Ciencia Project CTQ2004-01739 (Spain), Generalitat Valenciana Project GV06/192, and the European Regional Development Fund.

1. Daniels, M. & Hauswirth, W. (1971) *Science* **171,** 675–676.
2. Crespo-Hernández, C. E., Cohen, B., Hare, P. M. & Kohler, B. (2004) *Chem. Rev.* **104,** 1977–2019.
3. Nordlund, T. M., Andersson, S., Nilsson, L., Rigler, R., Gräslund, A. & McLaughlin, L. W. (1989) *Biochemistry* **29,** 9095–9103.
4. Guest, C. R., Hochstrasser, R. A., Sowers, L. C. & Millar, D. P. (1991) *Biochemistry* **30,** 3271–3279.
5. Bloom, L. B., Otto, M. R., Beechem, J. M. & Goodman, M. F. (1993) *Biochemistry* **32,** 11247–11258.
6. Rachofski, E. L., Osman, R. & Ross, J. B. A. (2001) *Biochemistry* **40,** 946–956.
7. O'Neill, M. A. & Barton, J. K. (2002) *J. Am. Chem. Soc.* **124,** 13053–13066.
8. Wassam, W. A. & Lim, E. C. (1978) *J. Chem. Phys.* **68,** 433–454.
9. Lim, E. C. (1977) in *Excited States*, ed. Lim, E. C. (Academic, New York).
10. Lim, E. C. (1986) *J. Phys. Chem.* **90,** 6770–6777.
11. Broo, A. (1998) *J. Phys. Chem.* **102,** 526–531.
12. Rachofsky, E. L., Ross, J. B. A., Krauss, M. & Osman, R. (2001) *J. Phys. Chem. A* **105,** 190–197.
13. Mennucci, B., Toniolo, A. & Tomasi, J. (2001) *J. Phys. Chem. A* **105,** 4749–4757.
14. Mennucci, B., Toniolo, A. & Tomasi, J. (2001) *J. Phys. Chem. A* **105,** 7126–7134.
15. Marian, C. M., Schneider, F., Kleinschmidt, M. & Tatchen, J. (2002) *Eur. Phys. J. D* **20,** 357–367.
16. Domke, W., Yarkony, D. R. & Köppel, H., eds. (2004) *Conical Intersections* (World Sci., Singapore).
17. Olivucci, M., ed. (2005) *Computational Photochemistry* (Elsevier, Amsterdam).
18. Klessinger, M. & Michl, J. (1995) *Excited States and Photochemistry of Organic Molecules* (VCH, New York).
19. Köppel, H., Domcke, W. & Cederbaum, L. S. (1984) *Adv. Chem. Phys.* **57,** 59–246.
20. Robb, M. A., Olivucci, M. & Bernardi, F. (1998) in *Encyclopedia of Computational Chemistry*, eds. Schlegel, P. v. R., Schreiner, P. R., Schaefer, H. F., III, Jorgensen, W. L., Thiel, W. & Glen, R. C. (Wiley, Chichester, U.K.).
21. Yarkony, D. R. (1995) in *Modern Electronic Structure Theory*, ed. Yarkony, D. R. (World Sci., Singapore), Part 1.
22. Chachisvilis, M. & Zewail, A. H. (1999) *J. Phys. Chem. A* **103,** 7408–7418.
23. Pecourt, J. –M. L., Peon, J. & Kohler, B. (2000) *J. Am. Chem. Soc.* **122,** 9348–9349.
24. Zimmerman, H. E. (1966) *J. Am. Chem. Soc.* **88,** 1566–1567.
25. Michl, J. (1972) *Mol. Photochem.* **4,** 243–256.
26. Bernardi, F., Olivucci, M. & Robb, M. A. (1995) *Pure App. Chem.* **67,** 17–24.
27. Ismail, N., Blancafort, M., Olivucci, M., Kohler, B. & Robb, M. A. (2002) *J. Am. Chem. Soc.* **124,** 6818–6819.
28. Sobolewski, A. L., Domcke, W., Dedonder-Lardeux, C. & Jouvet, C. (2002) *Phys. Chem. Chem. Phys.* **4,** 1093–1100.
29. Sobolewski, A. L. & Domcke, W. (2003) *Eur. Phys. J. D* **20,** 369–374.
30. Merchán, M. & Serrano-Andrés, L. (2003) *J. Am. Chem. Soc.* **125,** 8108–8109.
31. Matsika, S. (2004) *J. Phys. Chem. A* **108,** 7584–7590.
32. Merchán, M., Serrano-Andrés, L., Robb, M. A. & Blancafort, L. (2005) *J. Am. Chem. Soc.* **127,** 182–1825.
33. Marian, C. M. (2005) *J. Chem. Phys.* **122,** 104314.
34. Perun, S., Sobolewski, A. L. & Domcke, W. (2005) *J. Am. Chem. Soc.* **127,** 6257–6265.
35. Serrano-Andrés, L., Merchán, M. & Borin, A. C. (2006) *Chem. Eur. J.*, in press.
36. Seefeld, K. A., Plützer, C., Löwenich, D., Häber, T., Linder, R., Kleinermanns, K., Tatchen, J. & Marian, M. (2005) *Phys. Chem. Chem. Phys.* **7,** 3021–3026.
37. Ullrich, S., Schultz, T., Zgierski, M. Z. & Stolow, A. (2004) *J. Am. Chem. Soc.* **126,** 2262–2263.
38. Canuel, C., Mons, M., Pluzzi, F., Tardivel, B., Dimicoli, I. & Elhanine, M. (2005) *J. Chem. Phys.* **122,** 074316.
39. Holmen, A., Nordén, B. & Albinsson, B. (1997) *J. Am. Chem. Soc.* **119,** 3114–3121.
40. Santhosh, C. & Mishra, P. C. (1991) *Spectrochim. Acta* **47,** 1685–1693.
41. Pal, S. K., Peon, J. & Zewail, A. H. (2002) *Chem. Phys. Lett.* **363,** 57–63.
42. Fiebig, T., Wan, C. & Zewail, A. H. (2002) *ChemPhysChem* **3,** 781–788.
43. Neely, R. K., Magennis, S. W., Dryden, D. T. F. & Jones, A. C. (2004) *J. Phys. Chem. B* **108,** 17606–17610.
44. Somsen, O. J. G., van Hoek, A. & van Amerongen, H. (2005) *Chem. Phys. Lett.* **402,** 61–65.
45. Ward, D. C., Reich, E. & Stryer, L. (1969) *J. Biol. Chem.* **244,** 1228–1237.
46. Callis, P. R. (1979) *Chem. Phys. Lett.* **61,** 563–567.
47. Callis, P. R. (1983) *Ann. Rev. Phys. Chem.* **34,** 329–357.
48. Cohen, B., Hare, P. M. & Kohler, B. (2003) *J. Am. Chem. Soc.* **125,** 13594–13601.
49. Vigny, P. & Duquesne, M. (1977) in *Organic Molecular Photophysics*, ed. Birks, J. B. (Wiley, New York), pp. 167–177.
50. Jonas, I. & Michl, J. (1978) *J. Am. Chem. Soc.* **100,** 6834–6838.
51. Morgan, J. P. & Daniels, M. (1979) *Chem. Phys. Lett.* **67,** 533–537.
52. Nir, E., Keinermanns, K., Grace, L. & De Vries, M. S. (2001) *J. Phys. Chem. A* **105,** 5106–5110.
53. Platt, J. R. (1949) *J. Chem. Phys.* **17,** 484–495.
54. Plützer, C., Nir, E., de Vries, M. S. & Kleinermanns, K. (2001) *Phys. Chem. Chem. Phys.* **3,** 5466–5469.
55. Kim, N. J., Jeong, G., Kim, Y. S., Sung, J., Kim, S. K. & Park, Y. D. (2000) *J. Chem. Phys.* **113,** 10051–10055.
56. Lührs, D. C., Viallon, J. & Fischer, I. (2001) *Phys. Chem. Chem. Phys.* **3,** 1827–1831.
57. Nir, E., Plutzer, C., Kleinermanns, K. & De Vries, M. S. (2002) *Eur. Phys. J. D* **20,** 317–329.
58. Kim, N. J., Kang, H., Park, Y. D. & Kim, S. K. (2004) *Phys. Chem. Chem. Phys.* **6,** 2802–2805.
59. Clark, L. B., Peschel, G. G. & Tinoco, I. (1965) *J. Phys. Chem.* **69,** 3615–3618.
60. Sutherland, J. C. & Griffin, K. (1984) *Biopolymers* **23,** 2715–2724.
61. Fülscher, M. P., Serrano-Andrés, L. & Roos, B. O. (1997) *J. Am. Chem. Soc.* **119,** 6168–6176.
62. Kang, H., Lee, K. T., Jung, B., Ko, Y. & Kim, S. K. (2002) *J. Am. Chem. Soc.* **124,** 12958–12959.
63. Kang, H., Jung, B. & Kim, S. K. (2003) *J. Chem. Phys.* **118,** 6717–6719.
64. Larsen, O. F. A., van Stokkum, I. H. M., Groot, M.-L., Kennis, J. T. M., van Grondelle, R. & van Amerongen, H. (2003) *Chem. Phys. Lett.* **371,** 157–163.
65. Andersson, K, Malmqvist, P.-Å., Roos, B. O., Sadlej, A. J. & Wolinski, K. (1990) *J. Phys. Chem.* **94,** 5483–5488.
66. Andersson, K., Malmqvist, P.-Å. & Roos, B. O. (1992) *J. Chem. Phys.* **96,** 1218–1226.
67. Serrano-Andrés, L., Merchán, M., Nebot-Gil, I., Lindh, R. & Roos, B. O. (2003) *J. Chem. Phys.* **98,** 3151–3162.
68. Roos, B. O., Andersson, K., Fülscher, M. P., Malmqvist, P.-Å., Serrano-Andrés, L., Pierloot, K. & Merchán, M. (1996) *Adv. Chem. Phys.* **93,** 219–331.
69. Serrano-Andrés, L. & Merchán, M. (2004) in *Encyclopedia of Computational Chemistry*, eds. Schlegel, P. v. R., Schreiner, P. R., Schaefer, H. F., III, Jorgensen, W. L., Thiel, W. & Glen, R. C. (Wiley, Chichester, U.K.).
70. Merchán, M. & Serrano-Andrés, L. (2005) in *Computational Photochemistry*, ed. Olivucci, M. (Elsevier, Amsterdam).
71. Serrano-Andrés, L., Merchán, M. & Lindh, R. (2005) *J. Chem. Phys.* **122,** 104107.
72. Andersson, K., Barysz, M., Bernhardsson, A., Blomberg, M. R. A., Carissan, Y., Cooper, D. L., Cossi, M., Fülscher, M. P., Gagliardi, L., de Graaf, C., *et al.* (2004) MOLCAS (University of Lund, Lund, Sweden), Version 6.0.
73. Strickler, S. J. & Berg, R. A. (1962) *J. Chem. Phys.* **37,** 814–822.